

## The mantle structure below petit-spot volcanoes

Naoto Hirano <sup>1</sup>✉ & Shiki Machida <sup>2</sup>✉

Petit-spot volcanoes provide a unique opportunity to directly examine the structure and geochemical composition of the lithospheric and asthenospheric mantle beneath the subducting oceanic crust. Currently, petit-spot volcanos—formed in response to the flexure of subducting oceanic plates—are known to exist off the Japan, Java, Chile and Mariana trenches, however, the difficulties associated with detecting them leaves the possibility that they may be more widespread along outer rise of plates. Investigation of the lavas and xenolithic material erupted from petit-spot volcanos has suggested that the suboceanic lithosphere is largely metasomatized by numerous ascending petit-spot melts. This somewhat contradicts previous understanding which indicated that the oceanic lithosphere has a depleted mantle composition. The ultimate source and geodynamic processes that lead to the formation of petit-spot melts remain ambiguous, however, possibilities include that the lavas originate from incipient asthenospheric carbonatitic or carbonated silicate melts that are characteristically depleted in zirconium and hafnium. Typical geochemical trends in petit-spot lava fields off Japan trench indicate elemental partitioning through the immiscible separation of carbonate and silicate melts.

**T**he dynamics of the Earth's interior are reflected in processes at the Earth's surface, where the rigid plates (lithosphere) experience stress as they move over the ductile asthenosphere. Direct observations of the petrology and geochemistry of the mantle below oceanic regions have been largely restricted to areas near mid-ocean ridges and hotspots. Hirano et al.<sup>1,2</sup> first observed petit-spot submarine volcanoes on the old Pacific Plate off the Japan Trench prior to subduction. They attributed the occurrence of petit-spot volcanoes to brittle fractures in the upper lithosphere caused by flexure of the old, cold lithosphere, through which incipient asthenospheric melts may be squeezed upward by tectonic forces associated with plate flexure.

The petrography of the lithospheric mantle below ocean has been well characterized only using the observations of abyssal peridotites and oceanic core complexes near spreading centers (i.e., mid-ocean ridges) and also in ophiolite sections<sup>3–5</sup>, recognized as a depleted section after the extraction of mid-oceanic ridge basalts. Furthermore, most xenoliths observed in hotspot lavas experienced metasomatism due to the ascending mantle plume and related melts prior to their entrainment<sup>6–8</sup>. However, some xenolithic and xenocrystic fragments in petit-spot magmas include lithospheric materials, representing the first known materials directly sampling the lithosphere below the abyssal plain far from oceanic islands, seamounts, and spreading centers. These samples thus provide a unique opportunity to directly examine the lithospheric mantle beneath the subducting oceanic crust in regions beyond mid-ocean ridges and hotspots.

Petit-spot melts are considered to originate in the asthenosphere because the concave flexure of the outer-rise lithosphere may promote melt ascent in the absence of any ascending mantle plume or hotspot<sup>1,9</sup>. Ascending petit-spot melts are also expected to contribute toward the understanding of asthenospheric components just below the lithosphere. Therefore, the geochemistry of petit-spot lavas and entrained xenoliths provide the first evidence of the structure and dynamics of the suboceanic upper mantle, which remained inaccessible prior to the

<sup>1</sup>Center for Northeast Asian Studies, Tohoku University, 41 Kawauchi, Aoba-ku, Sendai 980-8576, Japan. <sup>2</sup>Ocean Resources Research Center for Next Generation, Chiba Institute of Technology, 2-17-1 Tsudanuma, Narashino 275-0016, Japan. ✉email: [nhirano@tohoku.ac.jp](mailto:nhirano@tohoku.ac.jp); [shiki.machida@p.chibakoudai.jp](mailto:shiki.machida@p.chibakoudai.jp)

discovery of petit-spot volcanoes. Here, we review the structure and geochemical composition of the suboceanic lithosphere and asthenosphere below petit-spot volcanoes on subducting plates prior to subduction.

**Petit-spot volcanism.** Petit-spot volcanoes of the northwestern (NW) Pacific Plate were first recognized as monogenetic eruptions due to melt ascent along the zone of concave flexure of the outer rise prior to plate subduction, which are visualized as positive gravity anomalies in Fig. 1 because they are aligned perpendicular to the surficial stress field of the concavely flexed lithosphere (Fig. 2). The erupted melts probably originate from the base of the lithosphere<sup>1</sup>. Because petit-spot volcanoes are too small to be detected by satellite altimetry, their exploration requires research vessels equipped for shipboard acoustic multi-beam surveys<sup>10</sup>; the global distribution of submarine petit-spot volcanoes, therefore, remains poorly constrained. Previously, surveyed areas were limited to regions off the Japan Trench on the NW Pacific Plate; there, the eruptive ages of petit-spot volcanoes are widely scattered, representing monogenetic eruptions over a period of >9 million years (Myr) in a large area around the

hinge line of the concavely flexed outer-rise lithosphere (Fig. 1). Off the northeastern Japanese coast (Sites A–C; Fig. 1) these tiny volcanoes have only ever been observed in non-uniformly distributed clusters (Fig. 3). No evidence of volcanism has been observed in areas surrounding the petit-spot volcanic provinces (Sites A–C). This implies that, in addition to plate flexure, other local factors in the source region below the lithosphere or asthenosphere plausibly control the occurrence of petit-spot volcanic provinces, such as regional presence of recycle materials and supply carbon from the deep upper mantle as mentioned below<sup>11</sup>.

Since their discovery, petit-spot volcanoes have also been reported in concavely flexed zones off the Java<sup>12</sup>, Chile<sup>13</sup>, and Mariana<sup>14</sup> Trenches. The North American mid-Cretaceous kimberlite corridor along the concave flexure of the continental lithosphere was also suggested to be due to the west-dipping subduction of the North American Plate<sup>15</sup>. Many other examples have been proposed as possible petit-spot volcanoes, such that their occurrence may not be restricted to outer-rise lithospheric warping prior to subduction. For example, the eruptive ages of western Samoan rejuvenated-stage lavas and surrounding small submarine volcanoes emplaced following the main shield-stage volcanism of the Samoan hotspot are geochronologically

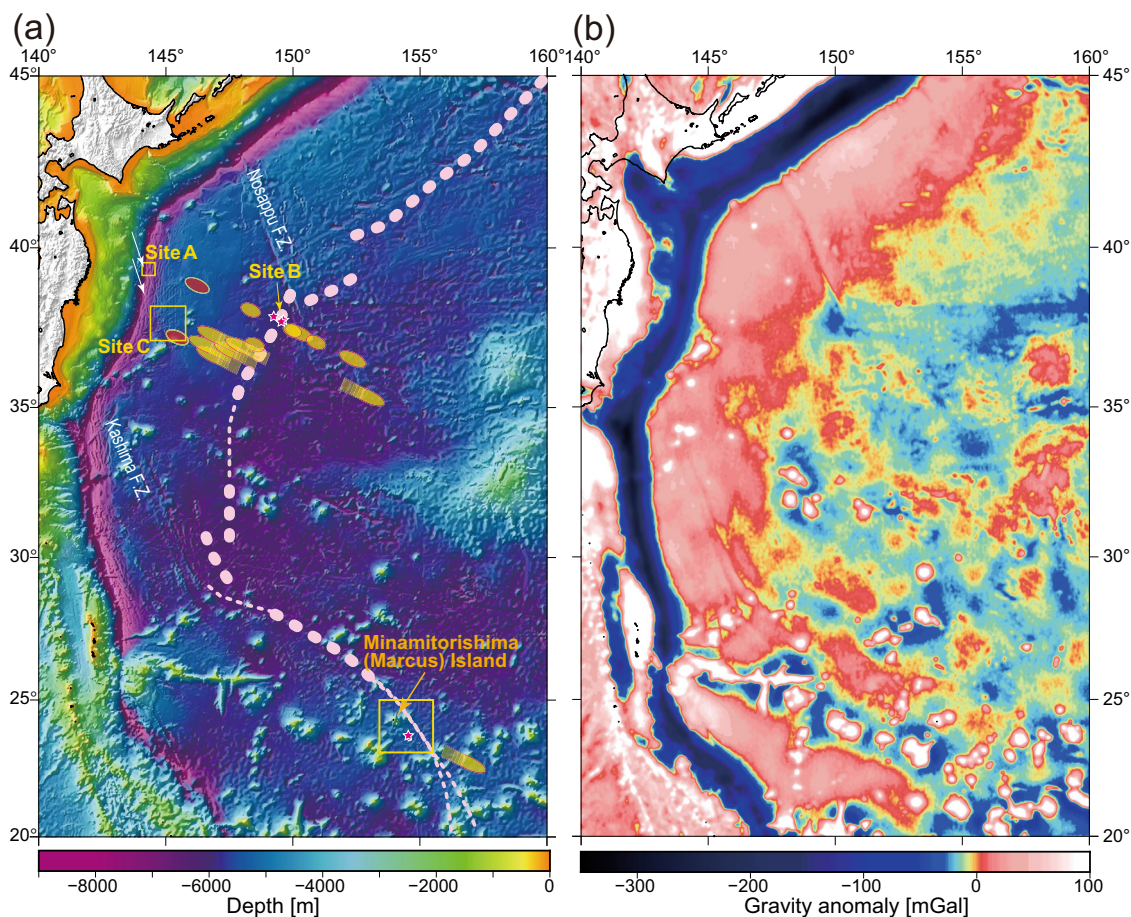


**Fig. 1 Bathymetry and marine gravity anomalies of the western part of the Pacific Plate.** Bathymetry (a) and marine gravity anomalies (b) are created using the data in ref. 72. Four petit-spot volcanic fields are here referred to as Sites A–C and SE of Minamitorishima Island; yellow squares indicate the areas shown in Fig. 3a, b (Sites A, C) and Fig. 3c (SE of Minamitorishima Island). Red ellipses filled with yellow indicate the approximate locations of petit-spot eruption estimated from the eruptive ages of the lavas and assuming constant plate motion at the present-day velocity ( $10.29 \text{ cm yr}^{-1}$ ; ref. 73)<sup>1,10,14,31,32,41</sup>; the two yellow ellipses filled with red atop the outer rise indicate DAP eruption sites. The thick dotted line in the left panel delineates the present hinge line of the concavely flexed outer rise of the western Pacific Plate trench-subduction systems, as defined by a gravity anomaly of  $-0 \text{ mGal}$  (right panel). Loading by seamount chains disturbs the positive gravity anomaly of the outer rise, as indicated by thin dotted lines. Small white arrows off NE Japan designate the azimuths of lithospheric structures on the oceanward slope of the trench that are sub-parallel to the neighboring Nosappu and Kashima Fracture Zones (‘F.Z.’)<sup>29</sup>.

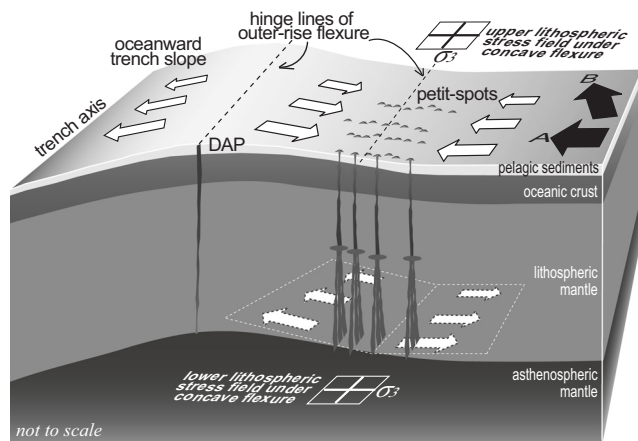


**Fig. 2 Tectonic model of magma ascent through the concavely flexed lithosphere.** White arrows indicate the stress fields at the base and surface of the lithosphere. Magmas ascend from a tensional stress field at the base of the lithosphere to a compressional stress field in the upper lithosphere; the least compressive principle stress ( $\sigma_3$ ) rotates by  $90^\circ$  at middle lithospheric depths. The two black arrows indicate plate motions in the cases of the Japan and Sunda Trenches (A) and the northern Mariana Trench (B) (modified after ref. 2).

consistent with tectonic uplift at the corner between a transform fault and the northern end of the Tonga Trench<sup>16</sup>. The alkaline and highly alkaline lavas erupted during the Hawaiian rejuvenated stage and in the North Arch volcanic field (a few hundred kilometers north of Oahu Island, Hawaii), which contrast with the main shield-stage lavas that abundantly erupt tholeiitic magmas, are also attributed to lithospheric flexure and decompression related to seamount/island loading, though they are also influenced by the Hawaiian plume<sup>17</sup>. However, other workers have attributed those occurrences to either the interaction of the ascending Hawaiian plume with asthenospheric convections or the presence of the Molokai Fracture Zone, not necessarily requiring lithospheric flexure<sup>18–20</sup>. Valentine and Hirano<sup>9</sup> concluded that the scattered distribution and small volumes of alkali basaltic volcanoes in the extensional Basin and Range, Nevada, North America, are analogous to petit-spot volcanism on the NW Pacific Plate. Uenzelmann-Neben et al.<sup>21</sup> suggested that volcanic eruptions off southern Greenland were due to glacial rebound of the lithosphere. Petit-spot basalts accreted into the Santa Rosa accretionary complex, Costa Rica, were erupted via intra-plate fissures in the paleo-Pacific basin<sup>22</sup>. Finally, Lindley<sup>23</sup> suggested the occurrence of petit-spot volcanoes in zones of plate-cracking along flexural ridge crests in the New Ireland Microplate. Whether occurring on the subducting outer rise or in intra-plate settings free of any mantle plumes and hotspots, petit-spot melts eventually escape to the surface.

**Subsurface structure of the subducting plate.** Submersible missions of Diving Support Vessel, *Shinkai 6500*, and Remote Operated Vessel, *Kaiko* near the axis of the Japan Trench observed petit-spot volcanic edifices truncated by normal faults of the subducting horst-and-graben structure on the oceanward slope of the trench. Petit-spot volcanoes consist of a volcanic cone built upon basement lava sheets<sup>1</sup>. The shipboard geophysical survey observed that volcanic sills beneath petit-spot edifices were mainly intruded at the base of the pelagic sediment column<sup>24</sup>. Moreover, the petit-spot volcanic field was recognized as an area of thin apparent sediment layers in the seismic reflection survey, implying the significant disturbance of sediment layer on the

incoming plate to the trench due to the petit-spot volcanic activities. Once subducted, the disturbed pelagic clays on the subducting slab associated with petit-spot volcanic fields are considered to be a factor controlling the hypocentral locations of interplate earthquakes<sup>25,26</sup>.

Hirano et al.<sup>1</sup> first proposed that incipient asthenospheric melts can be squeezed upward to the surface in response to tectonic forces (Fig. 2). The linear distributions of monogenetic petit-spot volcanoes in the volcanic fields near the axis of the Japan Trench (Site A; Fig. 3a) and in the offshore area at  $150^\circ\text{E}$  (Site B; red stars in Fig. 1) may correlate with the least compressive principal stress ( $\sigma_3$ ) on the concavely flexed outer rise because large lithospheric curvatures might result in brittle fractures in the upper lithosphere (Fig. 2). Indeed, an example of petit-spot volcanism off the Sunda Trench, a young dike intruded into the Late Cretaceous volcanic edifice of Christmas Island, is attributed to the concave flexure of the subducting outer rise<sup>12</sup>. In contrast, the distribution of more than 80 petit-spot volcanoes in the volcanic cluster at Site C, north of the Joban Seamounts in the NW Pacific Plate (Fig. 1), shows several alignments<sup>10</sup>: intersecting abyssal hills oriented parallel to the paleo-mid-ocean ridge, subparallel to fracture zone oriented perpendicular to the paleo-mid-ocean ridge, and subducting horst-and-graben structures<sup>27,28</sup> (Fig. 3b). The distribution of some young volcanic cones there seems to be controlled by the fabrics of ridge-parallel abyssal hills (lower panel, Fig. 3b), whereas most other lavas are distributed along ridge-perpendicular fabric zones that are sub-parallel to the neighboring Nosappu and Kashima Fracture Zones<sup>29</sup> (Figs. 1 and 3b). These observations show that, in general, petit-spot volcanoes are distributed along basement structures within the lithosphere, as well as along tectonic alignments of the flexed outer rise.

Western Pacific Plate petit-spot volcanoes SE of Minamitorishima (Marcus) Island (Fig. 1) also occur on the concavely flexed lithosphere of the outer rise of the Mariana Trench; there, the distance from the trench axis to the crest of the outer rise is the greatest among global subduction systems<sup>14,30</sup>. These volcanic edifices are more than 450 m high and, accounting for the long ridges that extend from the central cones, much more than 5 km across, slightly larger than those on the NW Pacific Plate. At least seven knolls in this field extend the ridges along N–S or NNE–SSW azimuths, subparallel to other nearby ridges (arrows in Fig. 3c). Because the hinge of the outer-rise flexure there is, exceptionally, subparallel to the plate motion, these alignments are roughly perpendicular to both the hinge line ( $\sigma_3$ ) and the plate motion (Figs. 1, 2 and 3a, c). Satellite-acquired gravity anomalies of the Nazca Plate off the Chile Trench indicate that two examples of Chilean petit-spot volcanic fields also erupted through the flexed lithosphere due to the subduction of the outer rise; there, however, flexure is also related to plate loading by the Juan Fernandez seamounts<sup>13</sup>.

**Melt ascent process.** Most NW Pacific Plate petit-spot lavas do not contain any phenocrysts, despite their fractionated compositions (45–52 wt%  $\text{SiO}_2$ ,  $\text{Mg}\# = 50\text{--}65$ , where  $\text{Mg}\# = 100 \times \text{Mg}/(\text{Mg} + \text{Fe})$ <sup>1,31–33</sup>, indicating that magmatic differentiation likely occurred in the magma chambers. Geobarometric data from lithospheric mantle xenoliths and xenocrysts indicate that the deepest-sourced peridotitic xenoliths derived from  $\sim 42$  km depth<sup>34</sup>, i.e., middle lithospheric depths corresponding to the region of elastic deformation<sup>35–38</sup>. These observations indicate that magmatic fractionation must have occurred at greater depths, such that the ascending magmas would have been stored at the depth of rotation of the  $\sigma_3$  stress axis from extension in the lower part of the concavely flexed lithosphere to compression in the upper part (Fig. 2). This rotation is the result of concave

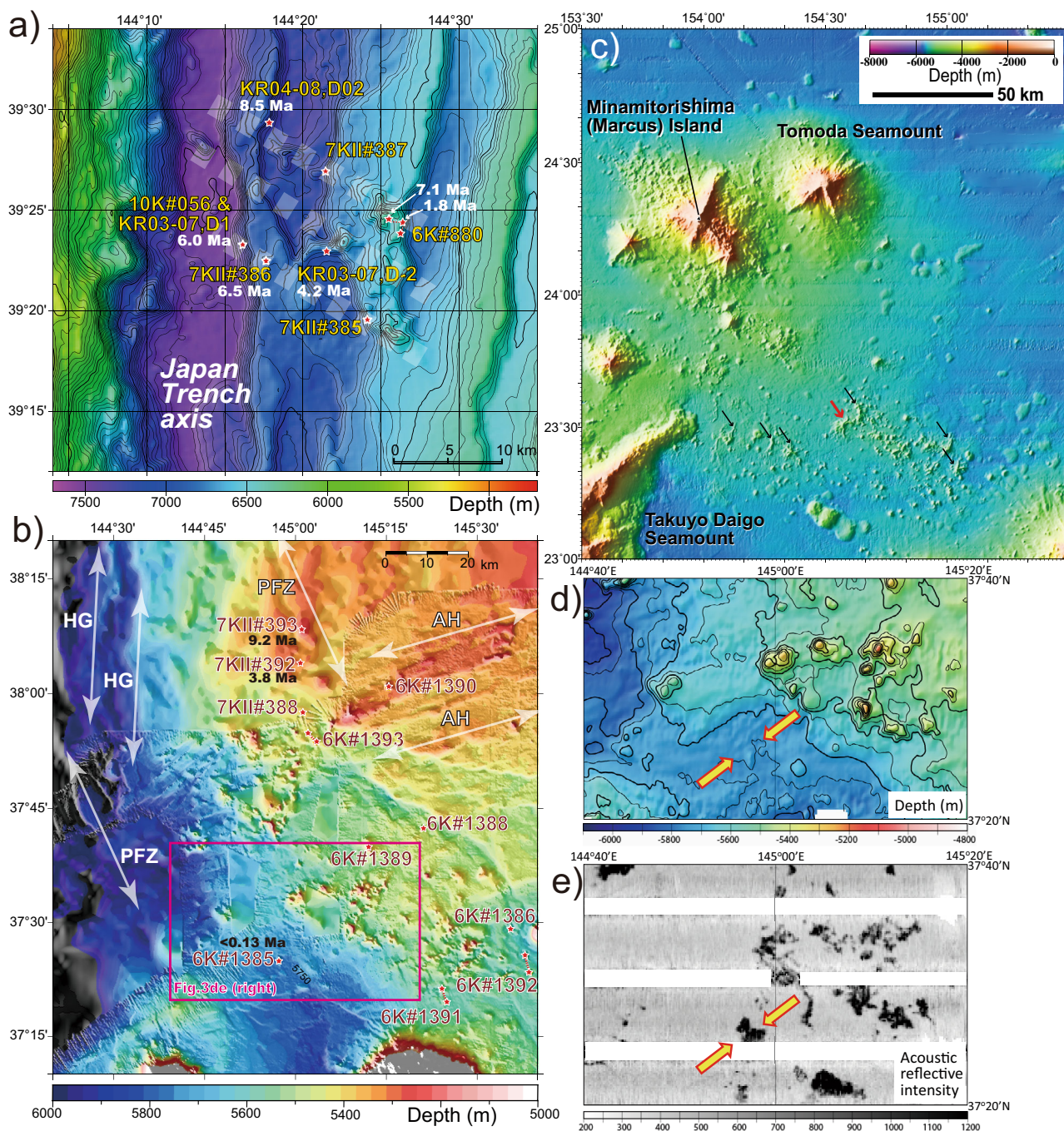


**Fig. 3 Detailed bathymetric maps.** **a** Sites A and **b** Site C in the NW Pacific Plate petit-spot volcanic field<sup>1</sup>, and **c** SE offshore of Minamitorishima Island in the western Pacific Plate<sup>14</sup> (see Fig. 1 for locations). Sampling sites are indicated by small red stars and eruptive ages are provided in **(a, b)**, when available<sup>1,10,31,32,41</sup>. Thick dashed lines in the panel **a** indicate lineations of monogenetic petit-spot volcanoes. In the panel **b**, white arrows designate lithospheric structures: AH, abyssal hills; PFZ, subparallel to fracture zone; and HG, horst and graben<sup>27–29</sup>. Young lavas, less than 3 Ma, are indicated by the red arrow in the panel **c**<sup>14</sup>. Black arrows in the panel **c** denote ridges aligned N-S to NNE-SSW in response to the flexure or the outer rise of the western Pacific lithosphere (see also Fig. 2). Detailed bathymetric and acoustic reflective maps around the volcanic field of DAP are shown in **(d, e)**, respectively<sup>10</sup> (red square in the panel **b**). The location of DAP is designated by thick yellow arrows.

flexure oceanward of the outer rise<sup>9</sup>. The ascent of NW Pacific Plate petit-spot melts is thus coherently explained by xenolith geobarometry, magmatic fractionation, and lithospheric stress fields, excluding two examples of the directly ascending petit-spots (DAPs) discussed below.

Recent research on the geochemistry of NW Pacific Plate petit-spot lavas and the petrography of xenoliths within them indicates that the conventional view of the lithosphere as a depleted

component requires some revision in terms of the nature of the subducting lithosphere. As a petit-spot volcanic cluster of the area with a diameter of 30 km in the Japan Trench repeatedly erupted at 1.8, 4.2, 6.0, 6.5, and 8.5 Ma<sup>1,10,31</sup>, Pilet et al.<sup>39</sup> and Yamamoto et al.<sup>40</sup> have reported that xenoliths entrained from the lithospheric mantle were derived from a region metasomatized by multiple petit-spot melts prior to the ascent of their host magmas, implying the presence of “hidden” petit-spot melts that

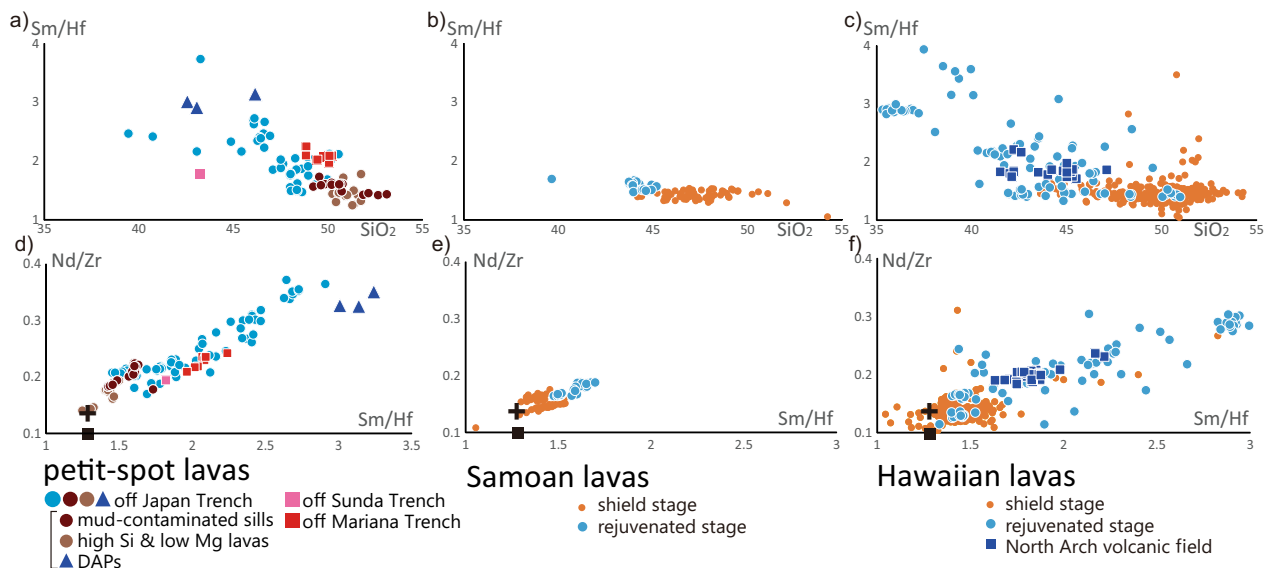


**Fig. 4** Geochemical compositions of petit-spot lavas and Samoan and Hawaiian lavas. Hawaiian lava compositions (**c, f**) are from the GeoRoc database (<http://georoc.mpch-mainz.gwdg.de/>)<sup>74</sup>. The representative N-MORB and OIB compositions are shown by the black square and cross, respectively<sup>75</sup>. Samoan lava compositions (**b, e**) are after ref. <sup>16</sup>. The data of petit-spot basalts (**a, d**) are available in Supplementary Data 1<sup>1,12,14,31,32</sup>. “Mud-contaminated sills” and “high Si & low Mg lavas” are described by “D02” and “G1c”<sup>31</sup>, respectively.

did not reach the surface (i.e., dikes or percolations into the lithospheric mantle). Indeed, cryptic metasomatic enrichments of clinopyroxenes in mantle xenoliths can be explained by metasomatic reaction with a primitive petit-spot melt composition<sup>39</sup>. The noble gas isotopic compositions of mantle xenoliths show diffusive He and Ar isotopic fractionations due to the migration of multiple petit-spot melts through the mantle<sup>40</sup>. These observations indicate that the lithospheric mantle in this region must have been significantly metasomatized prior to the onset of subduction in the Japan Trench. Otherwise, a depleted mantle component has been observed only in xenocrystic olivines (olivine Fo# = 90–92, indicating forsterite content in the olivine forsterite-fayalite solid solution series; coexisting chromian spinel Cr# = 0.5, where Cr# = Cr/(Cr + Al)) likely derived from the shallowest mantle<sup>33</sup>.

Two examples of petit-spot volcanoes erupted atop the outer rise at Site A and C in the NW Pacific Plate have been recognized as DAPs. Although a single outcrop was only found along the fault escarpment of trench oceanward slope at Site A, one at a southern area of Site C could be observed as a different complex from those of majority of other petit-spot volcanoes composed of knoll (a few hundred meters height and 1–2 km in diameter<sup>10</sup>). The DAP site seems to be composed of some flood lavas on an abyssal plain without knolls visualized only on the acoustic reflective intensity where it is difficult to find any morphologies in the shipboard bathymetry (Fig. 3d, e). The submersible dive observed pillow lava, tumuli, and hyaloclastites at a small mound (<30 m height and <1 km in diameter)<sup>41</sup>. DAPs show distinct melt ascent processes and magmatic compositions. Because the entire lithosphere below the summit of the outer rise is more extensional than at the base of the lithosphere, these melts can directly traverse the entire lithosphere (Fig. 2). The presence of both phenocrystic and xenocrystic olivines within the strongly alkaline DAP lavas (foidites) attests to their primitive composition (42–45 wt% SiO<sub>2</sub>) compared to the majority of petit-spot lavas (45–52 wt% SiO<sub>2</sub>)<sup>41</sup> (Fig. 4) (Supplementary Data 1). Silica-poor rejuvenated lavas erupted on western Samoa and part of Tutulia Island (<45 wt% SiO<sub>2</sub>; Fig. 4) occur in a similar tectonic setting; these DAP melts ascend due to the upward flexure of the

lithosphere at the corner of a transform fault and the northern end of the Tonga Trench<sup>16</sup>.

**Potential source of petit-spot melts.** The erupted lavas are usually highly vesicular, despite emerging under high hydrostatic pressures at 5–6 km below sea level<sup>1</sup>. The high vesicularity of petit-spot lavas is caused by the presence of up to 10 wt% of CO<sub>2</sub> in the magma<sup>42</sup>. Hirano et al.<sup>14</sup> noticed that, similar to western Pacific Plate petit-spot lavas, NW Pacific Plate petit-spot lavas are commonly depleted in Zr and Hf relative to other incompatible elements (Fig. 5), possibly reflecting a melt source in the garnet stability field of the carbonated mantle<sup>43</sup>. Here, we summarize the common geochemical features of Zr- and Hf-depleted lavas related to flexure of the oceanic lithosphere, i.e., global petit-spot lavas prior to subduction and rejuvenated-stage lavas erupted on the shield volcanic edifices of the Samoan and Hawaiian hotspots, including lavas of the submarine North Arch volcanic field (Fig. 4); Chilean petit-spot lavas are excluded from this comparison because they are highly influenced by the neighboring Juan Fernandez hotspot<sup>13,44</sup>. Lavas from mud-contaminated sills along the fault escarpment and a group of differentiated lavas have the highest SiO<sub>2</sub> contents and lowest Nd/Zr and Sm/Hf ratios of NW Pacific Plate petit-spot lavas<sup>1,31</sup>. The majority of the NW Pacific Plate petit-spot lavas have higher Sm/Hf and Nd/Zr ratios (i.e., Zr and Hf depletions) than Hawaiian and Samoan shield-stage lavas or the globally representative ocean island basalt (OIB) composition (Fig. 4).

The Zr and Hf anomalies of alkali-basaltic melts result from the reaction of orthopyroxene and silica-undersaturated melt to produce olivine and silica-rich melt<sup>45,46</sup>. This reaction is reasonable during the ascent of alkaline melts through the depleted lithospheric mantle; ultramafic xenoliths in NW Pacific Plate petit-spot lavas record the metasomatic reaction of early ascending petit-spot melts in the lithospheric mantle as enrichments of Zr and Hf in orthopyroxenes and light rare earth elements (REEs) in clinopyroxenes<sup>39</sup>. However, the negative correlation of SiO<sub>2</sub> content and Sm/Hf for all lavas in Fig. 4 contradicts the consumption of orthopyroxene to produce silica-

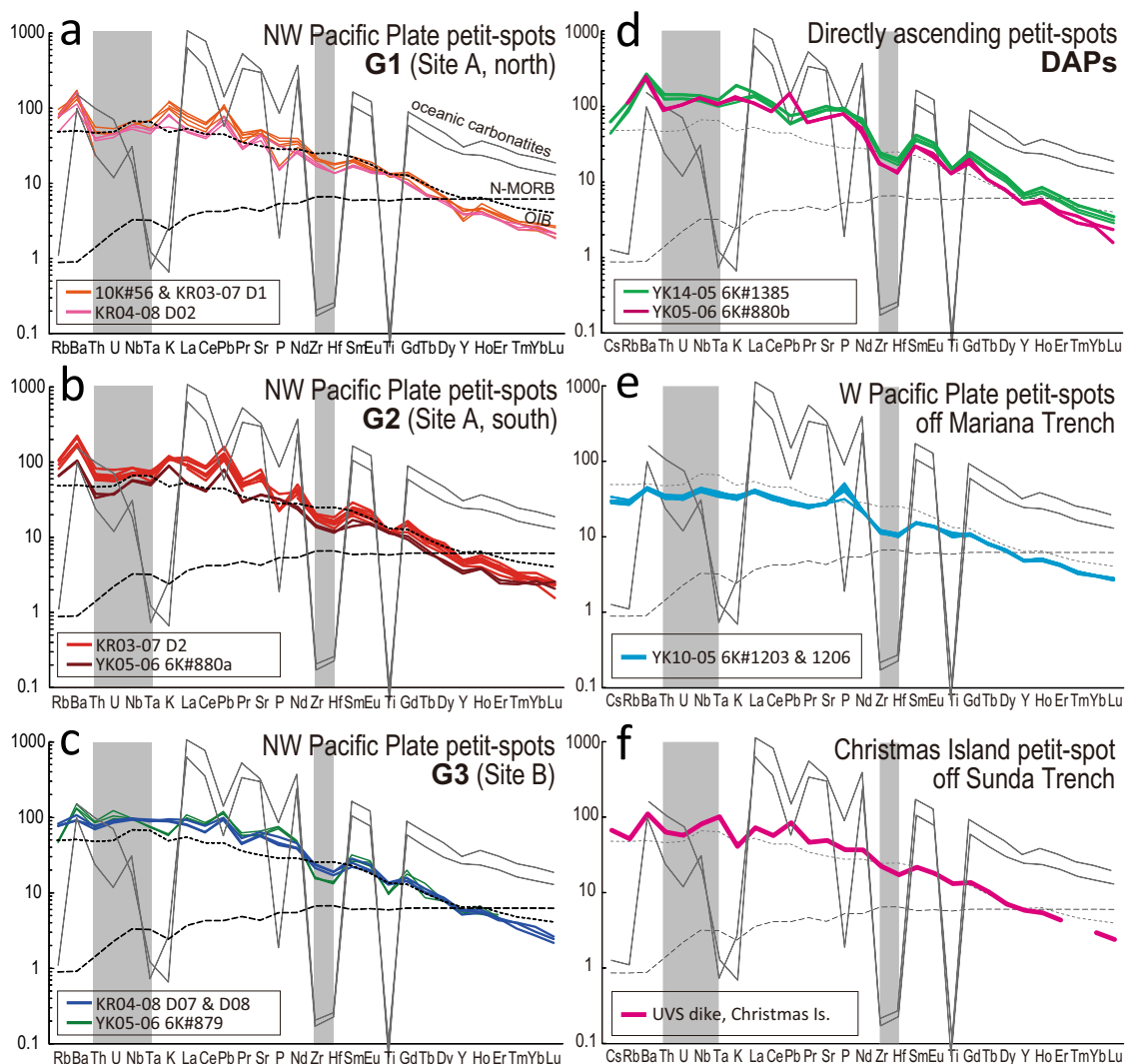


**Fig. 5** Geochemistry in incompatible elements normalized by primitive mantle (spidergram) of various petit-spot lavas. **a–d** NW Pacific Plate petit-spots, **e** western Pacific Plate petit-spots, and **f** Christmas Island petit-spot off Sunda Trench. The lavas on “oceanic carbonatite” show thin gray patterns<sup>76</sup>. The representative N-MORB and OIB compositions are broken and dotted lines, respectively<sup>75</sup>. Gray hatched bars correspond the compositions of Th, U, Nb, Ta, Zr, and Hf. Although the negative anomalies in Th, U, Nb, and Ta are mainly shown in G1 and G2 lavas of the NW Pacific Plate petit-spot, those in Zr and Hf are for all petit-spots as mentioned in Fig. 4. The data and the color legends are available in Supplementary Data 1.

rich melt. Instead, the presence of carbonated materials in the source region (as mentioned above) may be a main factor contributing to the observed Zr and Hf anomalies. In either case, petit-spot, North Arch, and rejuvenated-stage basalts can easily be discriminated from OIBs and are identified as alkaline (or strongly alkaline) lavas related to lithospheric flexure and depleted in Zr and Hf relative to other incompatible elements (Fig. 4) because of their source compositions, plausibly affected by a carbonatitic component.

**Test of carbonatite–silicate immiscibility.** The NW Pacific Plate petit-spot basalts are characteristically enriched in alkaline elements (Na<sub>2</sub>O and K<sub>2</sub>O) and highly incompatible elements such as Ba, Rb, U, Th, Nb, Ta, and light REEs<sup>1,31</sup>, comparable to the silica-undersaturated alkaline rocks that often accompany carbonatite magmas<sup>47–49</sup>. Based on ratios (e.g., Ba/Nb, Sm/Hf) of elements preferentially incorporated into carbonatite (Nb, Hf) or silicate melts (Ba, Sm) and Sr–Nd isotopic compositions, Machida et al.<sup>31</sup> classified these basalts into three groups: G1 (negative anomalies of U, Th, Nb, and Ta, and slight negative anomalies of

Zr and Hf), G2 (apparent negative anomalies of U, Th, Nb, Ta, Zr, and Hf), and G3 (negative anomalies of only Zr and Hf) (Fig. 5). These groups are further subdivided into G1a (basaltic trachyandesite), G2a (trachybasalt), and G1b, G2b, and G3 (basanite) based on their bulk compositions<sup>31</sup>. We selected representative, relatively primary (i.e., lower FeO\*/MgO) G1 and G2 basalt compositions to estimate elemental partitioning during carbonatite–silicate immiscibility.

To test whether liquid immiscibility experienced by the magmas before their eruption, we focused on elemental partitioning trends during the immiscible separation of carbonate and silicate melts<sup>50</sup> and on the correlation between the partitioning of Ca and REEs<sup>51</sup>. Martin et al.<sup>50</sup> reported characteristic correlations between the carbonate–silicate melt partition coefficients<sup>50–54</sup> ( $D^{\text{carbonate melt/silicate melt}}$ ; hereafter, simply  $D$ ) and ionic potentials of different elements. In particular, the  $D$  values for REEs, Th, Zr, and Hf changed systematically with the degree polymerization (i.e., as the number of non-bridging oxygens per tetrahedrally coordinated cation, NBO/T), alkalinity (K<sub>2</sub>O/Na<sub>2</sub>O), and H<sub>2</sub>O content of silicate melt (see Supplementary Information for detailed review).

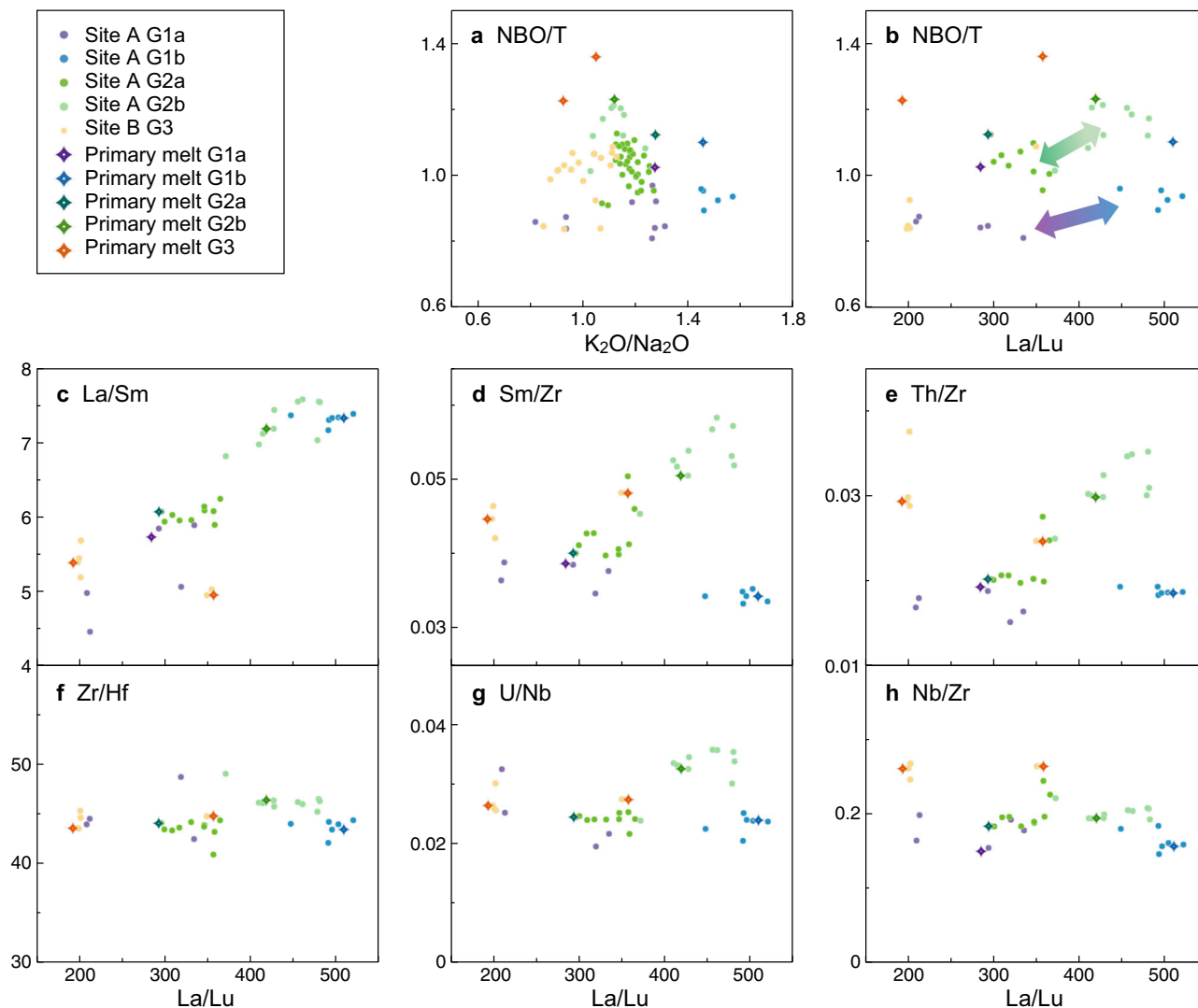


**Fig. 6 Variations of elemental ratios and NBO/T to be key of verification for trace-element partitioning by carbonatite-silicate immiscible melt separation.** Diagrams show a correlation between Alkalinity ( $K_2O/Na_2O$ ) (a) or La/Lu (b) and the degree of polymerization (NBO/T), and the trace-element ratios (c–h) of the primary magma calculated in this study and for the actual primitive petit-spot basalt samples from Site A<sup>31</sup>. Compositions of the “Primary melts” for each subgroups of G1 and G2 basalts and trace element compositions of G3 basalts were calculated on the basis of the actual samples as listed in Supplementary Table 1. Major element composition of the “Primary melts” for G3 basalts are from Machida et al.<sup>55</sup>. The thick arrows in (b) show the positive correlations in G1 and G2 basalts, respectively. The numerator of each trace-element ratio corresponds to the element with a lower ionic potential and the denominator to a higher ionic potential. The NBO/T was calculated on the basis of the strategy proposed by Mysen and Richet<sup>77</sup>.

The  $D^{REE}$  values calculated for all relatively hydrous (2.72–3.25 wt%  $H_2O$ ) primary petit-spot melts with  $K_2O/Na_2O > 1$  were greater than unity (Supplementary Table 1). This result is consistent with partitioning previously reported in the literature<sup>50,51</sup>, particularly for  $H_2O$ -bearing systems (Supplementary Fig. S1a). Additionally, the correlation between NBO/T and  $K_2O/Na_2O$  (Fig. 6a) indicates that although the “a” subgroups had lower NBO/T values than the “b” subgroups for both the G1 and G2 basalts, the  $K_2O/Na_2O$  value of the primary G1a melt was lower than that of G1b whereas the  $K_2O/Na_2O$  value of G2a was higher than that of G2b. From Supplementary Fig. S1b and Supplementary Table 2 we recognized two characteristic features of the calculated  $D^{REE}$  values. First, primary G1a and G2a melts with lower NBO/T values had higher  $D^{La}/D^{Lu}$  values than G1b and G2b melts, which had higher NBO/T values. Second, the differences of the  $D^{REE}$  values between subgroups G1a and G1b were smaller than those between subgroups G2a and G2b. The former feature indicates that the gradient of the inverse

correlation between  $D$  and ionic potential became steeper as melt polymerization increased. In contrast, the latter can be explained by the fact that the  $D^{REE}$  values of G1b basalts increased because of their higher  $K_2O/Na_2O$  values compared to G1a, which is not the case for G2 basalts (Fig. 6a). Therefore, we consider that these calculated  $D^{REE}$  values and tendencies are reasonable.

Based on partitioning systematics<sup>50</sup>, the ratios of lower- to higher-ionic-potential elements (i.e., La/Lu, Sm/Zr, Th/Zr, and Zr/Hf) of silicate melt to be useful indicators of carbonatite-silicate melt immiscibility (see Supplementary Information for detail). The overall positive correlation between La/Lu and NBO/T in each primary melt group (i.e., the La/Lu and NBO/T values of the “b” subgroups are higher than those of the “a” subgroups; thick arrows in Fig. 6b) can be explained by REE partitioning systematics during the immiscible separation of the carbonatite and silicate melts. Indeed, these tendencies are observed as intergroup variations among actual primitive basalt

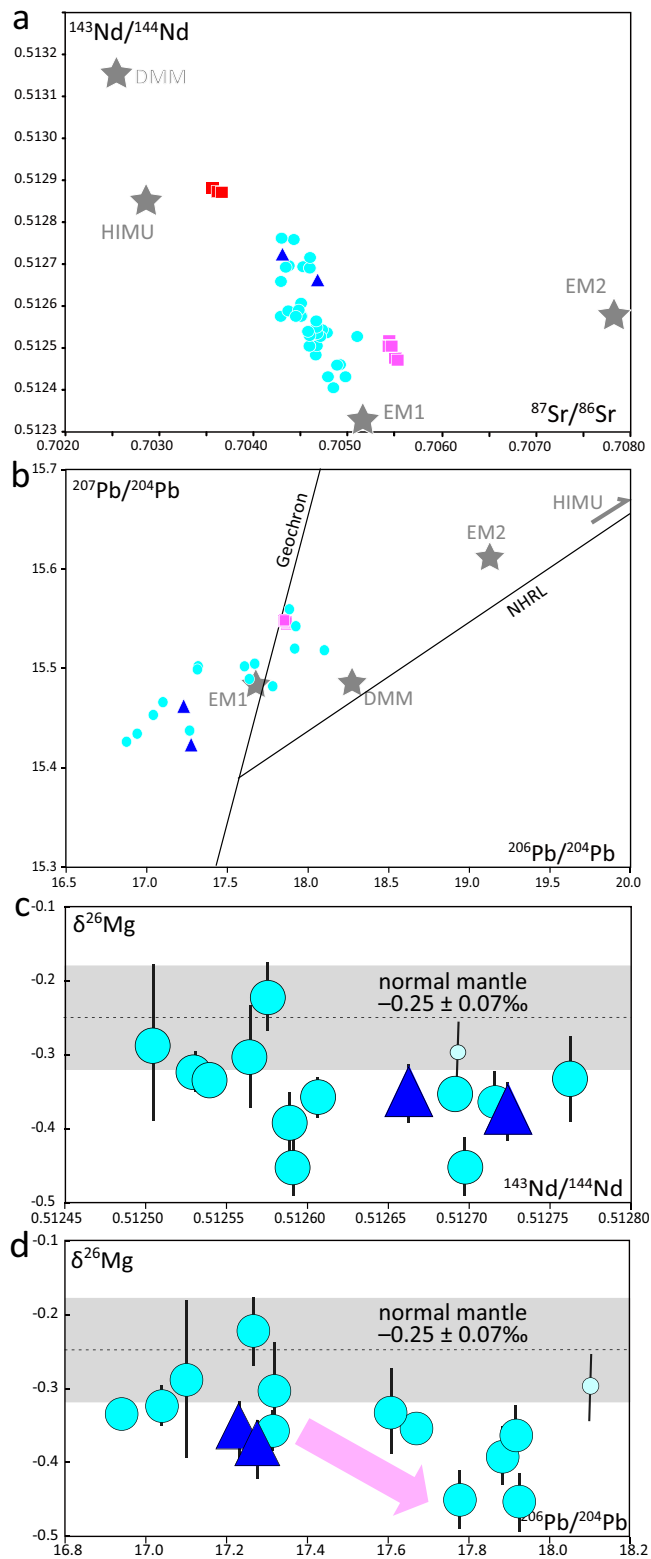


**Fig. 7 Isotopic composition of petit-spot basalts.** **a**  $^{87}\text{Sr}/^{86}\text{Sr}$  v.s.  $^{143}\text{Nd}/^{144}\text{Nd}$  ratios, **b**  $^{206}\text{Pb}/^{204}\text{Pb}$  v.s.  $^{207}\text{Pb}/^{204}\text{Pb}$  ratios, **c**  $^{143}\text{Nd}/^{144}\text{Nd}$  ratio v.s.  $\delta^{26}\text{Mg}$ , and **d**  $^{206}\text{Pb}/^{204}\text{Pb}$  v.s.  $\delta^{26}\text{Mg}$ . Right blue circles show the petit-spot basalt of NW Pacific Plate. Blue triangles show the DAP basalt. Red and pink colored squares show the petit-spot basalts off Mariana and Sunda trench, respectively. Mantle endmembers are DMM (Depleted Mid-ocean ridge basalt Mantle), EM-1 and EM-2 (Enriched Mantle 1, 2), and HIMU (High- $\mu$ )<sup>78–80</sup>. NHRL shows Northern Hemisphere Reference Line. A small circle in the panels **c**, **d** showing high  $\text{TiO}_2$  sample is omitted from discussion of the Mg isotopic composition. Error bars in **c**, **d** represent 2 standard deviations. The data are available in Supplementary Data 1.

among the subgroups of the G1 and G2 basalts, which were controlled by the degree of silicate melt polymerization and the proportions of silicate and carbonatite melts. The Zr and Nb enrichments (low Sm/Zr, Th/Zr, and U/Nb) of G1b basalts resulted from the low proportions of silicate melt and low  $D^{\text{Zr}}$  and  $D^{\text{Nb}}$  values (both <1; Supplementary Fig. S1a) compared to G1a basalts; Zr and Nb, being highly compatible with the silicate melt, were more effectively enriched in G1b basalts than Sm, Th, and U, which are compatible with the carbonatite melt ( $D^{\text{Sm}}$ ,  $D^{\text{Th}}$ ,  $D^{\text{U}} > 1$ ). In contrast, the  $D$  values in G2 primary melts were less variable (i.e., the slopes of the negative exponential correlations between  $D$  and ionic potential were gentler) and more elements must have been compatible with the silicate melt than in the G1 basalts (Supplementary Fig. S1a). Thus, the relative proportions of silicate melts in subgroup G2a were higher than those in G2b, and trace-element partitioning in the G2 primary melts was controlled solely by the segregation of the immiscible melts.

The G3 primary melts from Site B<sup>31,55</sup> were strongly silica-undersaturated. In contrast to G1 and G2 basalts, the trace-element ratios of the G3 primary melts and actual G3 basalt samples ( $\text{FeO}^*/\text{MgO} = 0.61\text{--}1.53$ ) were not systematically correlated with La/Lu or NBO/T (Fig. 6b–h). This result indicates that the geochemical features, particularly the trace-element systematics, of G3 basalts cannot be explained by partitioning during immiscible melt segregation. Indeed, previous experimental studies<sup>56,57</sup> observed only a single melt in this silica-undersaturated melt composition. Therefore, we assume that immiscibility did not develop during G3 volcanism.

**Implications for the geodynamic process producing petit-spot melts.**

$\text{CO}_2$ -rich incipient melts ascending from the asthenosphere are expected from experiment on  $\text{CO}_2$ -doped petit-spot melts last equilibrated with harzburgite at approximately 2 GPa and 1300 °C<sup>55</sup>. Indeed, Yamamoto et al.<sup>34</sup> estimated the melt porosity at the lithosphere-asthenosphere boundary (LAB) to be a few percent based on geothermobarometric measurements of xenoliths derived from the lithospheric mantle. The previously recognized continuous compositional variations of the basalt subgroups can be explained by the spatiotemporal evolution of the melt pond via a continuous melt supply, as discussed by Machida et al.<sup>31</sup>. Indeed, the relatively continuous but distinct compositional trends of La/Lu, La/Sm, Sm/Zr, Th/Zr, Zr/Hf, U/Nb, and Nb/Zr in the actual primitive basalt samples from each of the four subgroups (Fig. 6) indicate petrogenetically and temporally isolated magma systems corresponding to melt ponds at the LAB. Thus, we infer that immiscible melt separation occurred ubiquitously after the chemical evolution of the melt pond at the LAB. In contrast, the silica-undersaturated melts (G3 basalts) at Site B erupted onto the seafloor before reaching the solvus. Therefore, we conclude that the factors regulating the development of immiscibility were the chemical differences between the carbonate and silicate mantle materials and their varied mixing

samples  $\text{FeO}^*/\text{MgO} = 0.92\text{--}1.36$  for G1 basalts and  $0.78\text{--}1.08$  for G2 basalts (Fig. 6b). However, we also observed weak inverse correlations between La/Lu and NBO/T within the subgroups (particularly in subgroups G1a and G2a). The cause of this variation will be discussed in the next section.

The trends of the trace-element ratios (Fig. 6), including the negative correlations of Sm/Zr, Th/Zr, and U/Nb with La/Lu in each subgroup, can be explained by the differences in  $D$  values

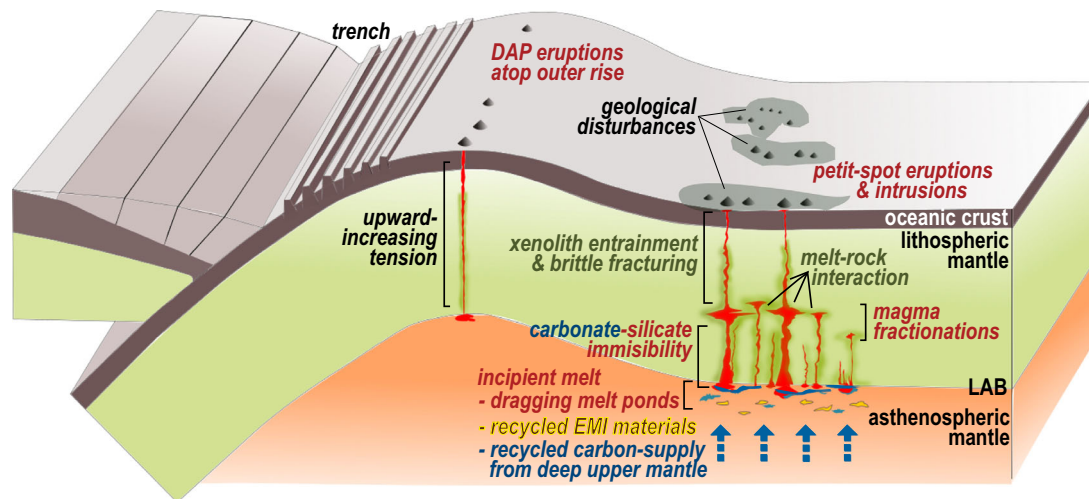


**Fig. 8 Schematic model of the formation and melt ascent processes of petit-spot and DAP volcanoes.** The majority of petit-spot melt at least plausibly ascend as carbonatitic melt after carbonate/silicate immiscibility. The melts excluding DAPs stack in the middle or lower asthenosphere. The sources are originated from asthenosphere with recycled materials.

proportions within the asthenosphere or LAB melt ponds. The individual trace-element compositions of the final silicate melts were therefore the result of elemental partitioning during immiscible melt segregation.

The occurrence of the LAB and the physical state of the asthenosphere, high electrical conductivity/anisotropy, and low seismic velocity below the LAB have remained enigmatic since the theory of plate tectonics was introduced (e.g., refs. 58,59). The solid-state deformation of the suboceanic asthenosphere has only ever been experimentally explained by the presence of hydrous olivine<sup>60</sup>, polycrystalline anelasticity<sup>61</sup>, and/or hydrous olivine creep<sup>62</sup> in the absence of partial melt. In contrast, depending on plate velocity and localized deformation, olivine could experience shear if the asthenosphere undergoes partial melting<sup>63</sup>. The presence of carbonatite or carbonated silicate melt has been proposed as a key in explaining the LAB and the electrical conductivity of the oceanic asthenosphere<sup>64,65</sup> because carbonated incipient melts can become fully interconnected along grain boundaries in the asthenospheric mantle at degrees of partial melting as low as 0.1%<sup>66</sup>. Such carbonated materials form low-degree partial melts in the asthenospheric peridotite matrix and can be stored at the LAB below the ocean<sup>64,65</sup>.

As mentioned above, the lack of volcanic activity in areas surrounding the NW Pacific Plate petit-spot volcanoes implies that a factor other than lithospheric flexure locally controls the occurrence of petit-spot volcanic provinces. Assuming that asthenospheric partial melts contain carbonatite or carbonated silicate, the depleted lithosphere might be ubiquitously metasomatized by veins of asthenospheric melt, corresponding to the lithospheric “hidden” petit-spots<sup>34,39</sup>. Alternatively, both solid-state deformation and local carbon doping by asthenospheric partial melts are plausible, the latter of which might be supplied by redox-melting below the asthenosphere<sup>11</sup>. Based on the interpretations of geochemistries and physical state of flexed lithosphere as mentioned above, we infer that ascending carbonatitic melt from asthenosphere probably stacked in the middle or lower asthenosphere after carbonate/silicate immiscibility at least for the majority of petit-spot melt, though this hypothesis requires further study.

Another important geochemical features of NW Pacific Plate petit-spot melts are the enriched mantle 1 (EM1) isotopic signatures of their lavas (low <sup>143</sup>Nd/<sup>144</sup>Nd ratios at a given <sup>87</sup>Sr/<sup>86</sup>Sr value and high <sup>208</sup>Pb/<sup>204</sup>Pb ratios at a given <sup>206</sup>Pb/<sup>204</sup>Pb value)<sup>16,31,67</sup> (Fig. 7a, b) and abnormally low  $\delta^{26}\text{Mg}$  values<sup>11</sup>

(Fig. 7c, d). Reinhard et al.<sup>16</sup> suggested that the EM1 isotopic signature is common to both Samoan rejuvenated-stage lavas and to petit-spot lavas of the NW Pacific Plate and Christmas Island (Indian Plate) related to tectonic uplift oceanward of subduction zones. Abnormally lower  $\delta^{26}\text{Mg}$  values of NW Pacific Plate petit-spot lavas (−0.25 to −0.45, including DAPs) than those of the typical mantle (uniform value of  $-0.25 \pm 0.07$ ) are correlated with the high-<sup>206</sup>Pb/<sup>204</sup>Pb end member, which is consistent with the subducted eclogite/pyroxenite against simple derivation from a DMM source with  $\delta^{26}\text{Mg}$  of  $\approx -0.25 \pm 0.07\text{‰}$  (Fig. 7c, d). The isotopic signature of crustal recycling, however, is decoupled from the elemental ratios strongly indicating carbonatite or carbonated silicate (high Zr/Hf, Nb/Ta, and low Ti/Eu)<sup>11</sup>, implying the multiple source components both of recycled carbonate and silicate materials for the source of NW Pacific Plate petit-spot lavas each.

The carbonate component in petit-spot lavas might originate from metal carbonates or diamonds in the highly reducing deep upper mantle<sup>11,68</sup>. However, based on experiments on carbonate-silicate reactions, Hammouda et al.<sup>69</sup> proposed that a carbon-rich layer exists throughout the asthenosphere, possibly fed by global subduction processes, which might correspond to a hydrous transition zone as a potential supply base<sup>70</sup>. The carbon and noble gas isotopic ratios of single petit-spot volcano on the western Pacific Plate (southeast of Minamitorishima Island)<sup>14</sup> indicate contamination by crustal carbon via reactions with micritic marine sediments of the oceanic crust<sup>71</sup>; otherwise, in the case of NW Pacific Plate petit-spot lavas, Mg and Pb isotopic covariations with trace element ratios contradict any contamination by marine sediments<sup>11</sup>. The high CO<sub>2</sub> compositions of petit-spot lavas, therefore, raise the possibility that carbonate affects petit-spot source components and their melting, at least in the case of NW Pacific Plate petit-spot lavas.

Our results suggest that processes controlling the mantle structure below petit-spot volcanoes include (1) geological perturbations caused by the emplacement of petit-spot lavas prior to their subduction; (2) ascending melts repeatedly metasomatizing the lithosphere; (3) melts stagnating in the middle to lower lithosphere, except for DAP melts; (4) the development of carbonate-silicate immiscibility before or during melt ascent; and (5) the plausible recycling of carbonatite and silicate melts below the LAB as the origin of petit-spot melts (Fig. 8). The submarine environment and the subducting

lithosphere and underlying asthenosphere may thus be modified more extensively than previously recognized by submarine petit-spot volcanoes and melts just prior to subduction. Most importantly, if immiscibility indeed develops, some as yet undiscovered “missing” carbon must be stored somewhere in the geosphere and eventually released into the hydrosphere and atmosphere.

### Data availability

The data sets analyzed in this review are cited in the appropriate sections of the manuscript text and supplementary information.

Received: 19 September 2021; Accepted: 14 April 2022;

Published online: 11 May 2022

### References

- Hirano, N. et al. Volcanism in response to plate flexure. *Science* **313**, 1426–1428 (2006).
- Hirano, N. Petit-spot volcanism: A new type of volcanic zone discovered near a trench. *Geochem. J.* **45**, 157–167 (2011).
- Dick, H. J. B., Tivey, M. A. & Tucholke, B. E. Plutonic foundation of a slow-spreading ridge segment: Oceanic core complex at Kane Megamullion, 23°30'N, 45°20'W. *Geochem. Geophys. Geosyst.* <https://doi.org/10.1029/2007GC001645> (2008).
- Warren, J. M. Global variations in abyssal peridotite compositions. *Lithos* **248–251**, 193–219 (2016).
- Ohara, Y. The Godzilla Megamullion, the largest oceanic core complex on the earth: A historical review. *Island Arc* **25**, 193–208 (2015).
- Bizims, M., Salters, V. J. M., Garcia, M. O. & Norman, M. D. The composition and distribution of the rejuvenated component across the Hawaiian plume: Hf–Nd–Sr–Pb isotope systematics of Kaula lavas and pyroxenite xenoliths. *Geochem. Geophys. Geosyst.* **14**, 4458–4478 (2013).
- Jackson, M. G., Shirey, S. B., Hauri, E. H., Kurz, M. D. & Rizo, H. Peridotite xenoliths from the Polynesian Austral and Samoa hotspots: Implications for the destruction of ancient <sup>187</sup>Os and <sup>142</sup>Nd isotopic domains and the preservation of Hadean <sup>129</sup>Xe in the modern convecting mantle. *Geochim. Cosmochim. Acta* **185**, 21–43 (2016).
- Snortum, E., Day, J. M. D. & Jackson, M. G. Pacific lithosphere evolution inferred from Aitutaki mantle xenoliths. *J. Petrol.* **60**, 1753–1772 (2019).
- Valentine, G. & Hirano, N. Mechanisms of low-flux intraplate volcanic fields—Basin and Range (North America) and Northwest Pacific Ocean. *Geology* **38**, 55–58 (2011).
- Hirano, N., Koppers, A. A. P., Takahashi, A., Fujiwara, T. & Nakanishi, M. Seamounts, knolls, and petit spot monogenetic volcanoes on the subducting Pacific Plate. *Basin Res.* **20**, 543–553 (2008).
- Liu, J. et al. Melting of recycled ancient crust responsible for the Gutenberg discontinuity. *Nat. Commun.* **11**, 172 (2020).
- Taneja, R., Rushmer, T., Blichert-Toft, T., Turner, S. & O'Neill, C. Mantle heterogeneities beneath the Northeast Indian Ocean as sampled by intra-plate volcanism at Christmas Island. *Lithos* **262**, 561–575 (2016).
- Hirano, N. et al. Petit-spot lava fields off the central Chile trench induced by plate flexure. *Geochem. J.* **47**, 249–257 (2013).
- Hirano, N. et al. Petit-spot volcanoes on the oldest portion of the Pacific Plate. *Deep-Sea Res. Part I* **154**, 103142 (2019).
- Zhang, W., Johnston, S. T. & Currie, C. A. Kimberlite magmatism induced by west-dipping subduction of the North American plate. *Geology* **47**, 395–398 (2019).
- Reinhard, A. A. et al. “Petit spot” rejuvenated volcanism superimposed on plume-derived Samoan shield volcanoes: Evidence from a 645 m drill core from Tutuila Island, American Samoa. *Geochem. Geophys. Geosyst.* **20**, 1485–1507 (2019).
- Bianco, T. A., Ito, G., Becker, J. M. & Garcia, M. O. Secondary Hawaiian volcanism formed by flexural arch decompression. *Geochem. Geophys. Geosyst.* **6**, Q08009 (2005).
- Ribe, N. M. & Christensen, U. R. The dynamical origin of Hawaiian volcanism. *Earth Planet. Sci. Lett.* **171**, 517–531 (1999).
- Yamamoto, M. & Morgan, J. P. North Arch volcanic fields near Hawaii are evidence favouring the restite-root hypothesis for the origin of hotspot swells. *Terra Nova* **21**, 452–466 (2009).
- Ballmer, M. D., Ito, G., Hunen, J. van & Tackley, P. J. Spatial and temporal variability in Hawaiian hotspot volcanism induced by small-scale convection. *Nat. Geosci.* **4**, 457–460 (2011).
- Uenzelmann-Neben, G., Schmidt, D. N., Niessen, F. & Stein, R. Intraplate volcanism off South Greenland: Caused by glacial rebound? *Geophys. J. Int.* **190**, 1–7 (2012).
- Buchs, D. M. et al. Low-volume intraplate volcanism in the Early/Middle Jurassic Pacific basin documented by accreted sequences in Costa Rica. *Geochem. Geophys. Geosyst.* **14**, 1552–1568 (2013).
- Lindley, I. D. Plate flexure and volcanism: Late Cenozoic tectonics of the Tabar–Lihir–Tanga–Feni alkaline province, New Ireland Basin, Papua New Guinea. *Tectonophysics* **677–678**, 312–323 (2016).
- Fujiwara, T., Hirano, N., Abe, N. & Takizawa, K. Subsurface structure of the “petit-spot” volcanoes on the northwestern Pacific Plate. *Geophys. Res. Lett.* **34**, L13305 (2007).
- Fujie, G. et al. Spatial variations of incoming sediments at the northeastern Japan arc and their implications for megathrust earthquakes. *Geology* **48**, 614–619 (2020).
- Akizawa, N. et al. A direct evidence for disturbance of whole sediment layer in the subducting Pacific plate by petit-spot magma–water/sediment interaction. *Marine Geol.* **444**, 106712 (2022).
- Nakanishi, M. *Modern Approaches in Solid Earth Sciences* (eds Ogawa, Y., Anma, R. & Dilek, Y.) 1–38 (Springer, Netherlands, 2011).
- Boston, B., Moore, G. F., Nakamura, Y. & Kodaira, S. Outer-rise normal fault development and influence on near-trench décollement propagation along the Japan Trench, off Tohoku. *Earth Planet. Space* **66**, 135 (2014).
- Nakanishi, M. Topographic Expression of Five Fracture Zones in the Northwestern Pacific Ocean. In: *The Mesozoic Pacific: Geology, Tectonics, and Volcanism, Geophysical Monograph Series Vol. 77* (eds Pringle, M. S. et al.) 121–135 (American Geophysical Union, 1993).
- Caldwell, J. G., Haxby, W. F., Karig, D. E. & Turcotte, D. L. On the applicability of a universal elastic trench profile. *Earth Planet. Sci. Lett.* **31**, 239–246 (1976).
- Machida, S. et al. Petit-spot geology reveals melts in upper-most asthenosphere dragged by lithosphere. *Earth Planet. Sci. Lett.* **426**, 267–279 (2015).
- Hirano, N., Kawamura, K., Hattori, M., Saito, K. & Ogawa, Y. A new type of intra-plate volcanism; young alkali basalts discovered from the subducting Pacific Plate, northern Japan Trench. *Geophys. Res. Lett.* **28**, 2719–2722 (2001).
- Hirano, N., Yamamoto, J., Kagi, H. & Ishii, T. Young, olivine xenocryst-bearing alkali-basalt from the oceanward slope of the Japan Trench. *Contrib. Mineral. Petrol.* **148**, 47–54 (2004).
- Yamamoto, J., Korenaga, J., Hirano, N. & Kagi, H. Melt-rich lithosphere–asthenosphere boundary inferred from petit-spot volcanoes. *Geology* **42**, 967–980 (2014).
- Shito, A., Suetsugu, D., Furumura, T., Sugioka, H. & Ito, A. Small-scale heterogeneities in the oceanic lithosphere inferred from guided waves. *Geophys. Res. Lett.* **40**, 1708–1712 (2013).
- Baba, K. et al. Is the electrical conductivity of the northwestern Pacific upper mantle normal? *Geochem. Geophys. Geosyst.* **14**, 4969–4979 (2013).
- Kawakatsu, H. & Utada, H. Seismic and electrical signatures of the lithosphere–asthenosphere system of the normal oceanic mantle. *Ann. Rev. Earth Planet. Sci.* **45**, 139–167 (2017).
- Rychert, C. A., Harmon, N., Constable, S. & Wang, S. The nature of the lithosphere–asthenosphere boundary. *J. Geophys. Res., Solid Earth* **125**, e2018JB016463 (2020).
- Pilet, S. et al. Pre-subduction metasomatic enrichment of the oceanic lithosphere induced by plate flexure. *Nat. Geosci.* **9**, 898–903 (2016).
- Yamamoto, J., Hirano, N., Abe, N. & Hanyu, T. Noble gas isotopic compositions of mantle xenoliths from northwestern Pacific lithosphere. *Chem. Geol.* **268**, 313–323 (2009).
- Sato, Y. et al. Direct ascent to the surface of asthenospheric magma in a region of convex lithospheric flexure. *Int'l Geol. Rev.* **60**, 1231–1243 (2018).
- Okumura, S. & Hirano, N. Carbon dioxide emission to Earth’s surface by deep-sea volcanism. *Geology* **41**, 1167–1170 (2013).
- Dasgupta, R., Hirschmann, M. M., McDonough, W. F., Spiegelman, M. & Withers, A. C. Trace element partitioning between garnet lherzolite and carbonatite at 6.6 and 8.6 GPa with applications to the geochemistry of the mantle and of mantle-derived melts. *Chem. Geol.* **262**, 57–77 (2009).
- Yamamoto, J., Hirano, N. & Kurz, M. D. Noble gas isotopic compositions of seamount lavas from the central Chile trench: Implications for petit-spot volcanism and the lithosphere asthenosphere boundary. *Earth Planet. Sci. Lett.* **552**, 116611 (2020).
- Shaw, C. S. J. Dissolution of orthopyroxene in basanitic magma between 0.4 and 2 GPa: Further implications for the origin of Si-rich alkaline glass inclusions in mantle xenoliths. *Contrib. Mineral. Petrol.* **135**, 114–132 (1999).
- Tamura, A., Arai, S., Takeuchi, M., Miura, M. & Pirnia, T. Compositional heterogeneity of a websterite xenolith from Kurose, southwest Japan: Insights into the evolution of lower crust beneath the Japan Arc. *Eur. J. Mineral.* **31**, 35–47 (2018).

47. Mourão, C. et al. Geochemical temporal evolution of Brava Island magmatism: Constraints on the variability of Cape Verde mantle sources and on carbonatite–silicate magma link. *Chem. Geol.* **334**, 44–61 (2012).
48. Weidendorfer, D., Schmidt, M. W. & Mattsson, H. B. Fractional crystallization of Si-undersaturated alkaline magmas leading to unmixing of carbonatites on Brava Island (Cape Verde) and a general model of carbonatite genesis in alkaline magma suites. *Contrib. Min. Petrol.* **171**, 43–46 (2016).
49. Dawson, J. B. Peralkaline nephelinite–natrocarbonatite relationships at Oldoinyo Lengai, Tanzania. *J. Petrol.* **39**, 2077–2094 (1998).
50. Martin, L. H. J., Schmidt, L. W., Mattsson, H. B. & Guenther, D. Element partitioning between immiscible carbonatite and silicate melts for dry and H<sub>2</sub>O-bearing systems at 1–3 GPa. *J. Petrol.* **54**, 2301–2338 (2013).
51. Nabyl, Z. et al. A window in the course of alkaline magma differentiation conducive to immiscible REE-rich carbonatites. *Geochim. Cosmochim. Acta* **282**, 297–323 (2020).
52. Hamilton, D. L., Bedson, P. & Esson, J. The Behaviour of Trace Elements in the Evolution of Carbonatites. In: *Carbonatites: Genesis and Evolution* (ed. Bell, K.), 405–427 (Unwin Hyman, Boston, 1989).
53. Veksler, I. V., Petibon, C., Jenner, G. A., Dorfman, A. M. & Dingwell, D. B. Trace element partitioning in immiscible silicate–carbonate liquid systems: An initial experimental study using a centrifuge autoclave. *J. Petrol.* **39**, 2095–2104 (1998).
54. Veksler, I. V. et al. Partitioning of elements between silicate melt and immiscible fluoride, chloride, carbonate, phosphate, and sulfate melts, with implications to the origin of natrocarbonatite. *Geochim. Cosmochim. Acta* **79**, 20–40 (2012).
55. Machida, S., Kogiso, T. & Hirano, N. Petit-spot as definitive evidence for partial melting in the asthenosphere caused by CO<sub>2</sub>. *Nat. Commun.* **8**, 14302 (2017).
56. Brooker, R. A. & Kjarsgaard, B. A. Silicate–carbonate liquid immiscibility and phase relations in the system SiO<sub>2</sub>–Na<sub>2</sub>O–Al<sub>2</sub>O<sub>3</sub>–CaO–CO<sub>2</sub> at 0.1–2.5 GPa with applications to carbonatite genesis. *J. Petrol.* **52**, 1281–1305 (2011).
57. Lee, W. J. & Wyllie, P. J. Liquid immiscibility in the join NaAlSi<sub>3</sub>O<sub>8</sub>–CaCO<sub>3</sub> to 2.5 GPa and the origin of calcic carbonatite magmas. *J. Petrol.* **37**, 1125–1152 (1996).
58. Gaherty, J. B., Kato, M. & Jordan, T. H. Seismological structure of the upper mantle: A regional comparison of seismic layering. *Phys. Earth Planet. Inter.* **110**, 21–41 (1999).
59. Karato, S. On the origin of the asthenosphere. *Earth Planet. Sci. Lett.* **321**–322, 95–103 (2012).
60. Faul, U. H. & Jackson, I. The seismological signature of temperature and grain size variations in the upper mantle. *Earth Planet. Sci. Lett.* **234**, 119–134 (2005).
61. Takei, Y. Effects of partial melting on seismic velocity and attenuation: A new insight from experiments. *Ann. Rev. Earth Planet. Sci.* **45**, 447–470 (2017).
62. Katsura, T. & Fei, H. Asthenosphere dynamics based on the H<sub>2</sub>O dependence of element diffusivity in olivine. *Nat'l Sci. Rev.* **8**, nwaa278 (2021).
63. Pommier, A. et al. Experimental constraints on the electrical anisotropy of the lithosphere–asthenosphere system. *Nature* **522**, 202–206 (2015).
64. Gaillard, F., Malki, F., Iacono-Marziano, G., Pichavant, M. & Scaillet, B. Carbonatite melts and electrical conductivity in the asthenosphere. *Science* **322**, 1363–1365 (2008).
65. Sifré, D. et al. Electrical conductivity during incipient melting in the oceanic low-velocity zone. *Nature* **509**, 81–85 (2014).
66. Gardés, E., Laumonier, M., Massuyeau, M. & Gaillard, F. Unravelling partial melt distribution in the oceanic low velocity zone. *Earth Planet. Sci. Lett.* **540**, 116242 (2020).
67. Machida, S., Hirano, N. & Kimura, J.–I. Evidence for recycled plate material in Pacific upper mantle unrelated to plumes. *Geochim. Cosmochim. Acta* **73**, 3028–3037 (2009).
68. Rohrbach, A. et al. Metal saturation in the upper mantle. *Nature* **449**, 456–458 (2007).
69. Hammouda, T. et al. Is there a global carbonate layer in the oceanic mantle? *Geophys. Res. Lett.* **48**, e2020GL089752 (2021).
70. Yang, J. & Feccenda, M. Intraplate volcanism originating from upwelling hydrous mantle transition zone. *Nature* **579**, 88–91 (2020).
71. Yamamoto, J., Kawano, T., Takahata, N. & Sano, Y. Noble gas and carbon isotopic compositions of petit-spot lavas from southeast of Marcus Island. *Earth Planet. Sci. Lett.* **497**, 139–148 (2018).
72. Sandwell, D. T., Müller, R. D., Smith, W. H. F., Garcia, E. & Francis, R. New global marine gravity model from CryoSat-2 and Jason-1 reveals buried tectonic structure. *Science* **346**, 65–67 (2014).
73. Gripp, A. E. & Gordon, R. G. Current plate velocities relative to the hotspots incorporating the NUVEL-1 global plate motion model. *Geophys. Res. Lett.* **17**, 1109–1112 (1990).
74. Sarbas, B., Jochum, K. P. & Nohl, U. GEOROC and GeoReM databases—linking chemical data and data quality. *Eos Transactions, American Geophysical Union* <http://georoc.mpch-mainz.gwdg.de/georoc/> Fall Meeting Supplement, Abstract IN23A-IN20957 (2007).
75. Sun, S.-S. & McDonough, W. F. Chemical and isotopic systematics of oceanic basalts: Implications for mantle composition and processes. *Geol. Soc. London, Spec. Publ.* **42**, 313–345 (1989).
76. Hoernle, K., Tilton, G., Le Bas, M. J., Duggen, S. & Garbe-Schönberg, D. Geochemistry of oceanic carbonatites compared with continental carbonatites: Mantle recycling of oceanic crustal carbonate. *Contrib. Mineral. Petrol.* **142**, 520–542 (2002).
77. Mysen, B. & Rickett, P. *Silicate glasses and melts* 2nd edn (Elsevier, 2019).
78. Hart, S.-R., Hauri, E. H., Oschmann, L. A. & Whitehead, J. A. Mantle plumes and entrainment: Isotopic evidence. *Science* **256**, 517–520 (1992).
79. Workman, R. K. & Hart, S. R. Major and trace element composition of the depleted MORB mantle (DMM). *Earth Planet. Sci. Lett.* **231**, 53–72 (2005).
80. Jackson, M. G. & Dasgupta, R. Compositions of HIMU, EM1, and EM2 from global trends between radiogenic isotopes and major elements in ocean-island basalts. *Earth Planet. Sci. Lett.* **276**, 175–186 (2008).

### Acknowledgements

We thank Oliver Nebel, Andrew Reinhard, and an anonymous reviewer for constructive reviews. We also thank Malcolm Massuyeau for critical suggestions to our evaluation of element partitioning between carbonate and silicate melts. Kazuto Mikuni and Yosuke Shimbo kindly supported this study by creating the geodynamic model and the geochemical database. This study was financially supported in part by the Toray Science and Technology Grant (#11–5208) and by the Japan Society for the Promotion of Science (#18H03733, 20K04098).

### Author contributions

N.H. proposed this review. N.H. and S.M. equally contributed to discussions of the manuscript scope and design.

### Competing interests

The authors declare no competing interests.

### Additional information

**Supplementary information** The online version contains supplementary material available at <https://doi.org/10.1038/s43247-022-00438-1>.

**Correspondence** and requests for materials should be addressed to Naoto Hirano or Shiki Machida.

**Peer review information** *Communications Earth & Environment* thanks Andrew Reinhard, Oliver Nebel, and the other, anonymous, reviewer(s) for their contribution to the peer review of this work. Primary Handling Editor: Joe Aslin. Peer reviewer reports are available.

**Reprints and permission information** is available at <http://www.nature.com/reprints>

**Publisher's note** Springer Nature remains neutral with regard to jurisdictional claims in published maps and institutional affiliations.



**Open Access** This article is licensed under a Creative Commons Attribution 4.0 International License, which permits use, sharing, adaptation, distribution and reproduction in any medium or format, as long as you give appropriate credit to the original author(s) and the source, provide a link to the Creative Commons license, and indicate if changes were made. The images or other third party material in this article are included in the article's Creative Commons license, unless indicated otherwise in a credit line to the material. If material is not included in the article's Creative Commons license and your intended use is not permitted by statutory regulation or exceeds the permitted use, you will need to obtain permission directly from the copyright holder. To view a copy of this license, visit <http://creativecommons.org/licenses/by/4.0/>.

© The Author(s) 2022